

Effects of the Lateral Ordering of Self-Assembled SiGe Nanoislands Grown on Strained $\text{Si}_{1-x}\text{Ge}_x$ Buffer Layers

V. V. Strelchuk^a, A. S. Nikolenko^a, P. M. Lytvyn^a, V. P. Kladko^a, A. I. Gudymenko^a, M. Ya. Valakh^a, Z. F. Krasilnik^b, D. N. Lobanov^b, and A. V. Novikov^b

^a*V. Lashkaryov Institute of Semiconductor Physics, National Academy of Sciences of Ukraine, Kyiv, 03028 Ukraine*

[^]*e-mail: nikolenko_mail@ukr.net*

^b*Institute for Physics of Microstructures, Russian Academy of Sciences, Nizhni Novgorod, 603950 Russia*

Submitted November 15, 2011; accepted for publication November 21, 2011

Abstract—Atomic-force microscopy, micro-Raman spectroscopy, and high resolution X-ray diffraction are applied to study the spatial ordering in single layers of SiGe nanoislands grown on a strained $\text{Si}_{1-x}\text{Ge}_x$ buffer sublayer. It is shown that, apart from stimulating the spatial ordering of nanoislands, the introduction of a $\text{Si}_{1-x}\text{Ge}_x$ sublayer leads to an enhanced role for interdiffusion processes. An unusually high increase in the volume of nanoislands in the process of the epitaxy is related to the anomalously strong diffusion from the buffer sublayer into the islands that is induced by nonuniform fields of elastic strains. The anisotropy of the islands shape and spatial ordering is discussed in terms of the anisotropy of the diffusion processes in spatially nonuniform fields of elastic strains.

DOI: 10.1134/S1063782612050211

1. INTRODUCTION

Controlling the size of semiconductor quantum dots (QDs), their size dispersion, and spatial ordering directly during the process of molecular-beam epitaxy is presently an issue of considerable importance [1]. It is known that spontaneous nucleation of coherent three-dimensional islands, which takes place after the formation of a homogeneous wetting layer (the Stranski–Krastanov mechanism), results in the chaotic mutual arrangement of QDs [2, 3]. Approaches aimed at improving spatial order in QD arrays and reducing the dispersion in QD size have included variation in the growth temperature and rate [4], making use of impurities and stressors to introduce centers for the nucleation of Ge islands on a Si substrate [5, 6], and growth on misoriented substrates [7, 8]. However, the problem of obtaining spatially ordered arrays of uniform Ge QDs is still a relevant one.

One possible way for solving this problem is the formation of spatially ordered dense arrays of GeSi islands on strained $\text{Si}_{1-x}\text{Ge}_x$ buffer sublayers. As shown previously [9, 10], the areal density of the islands increases with increasing Ge content in the $\text{Si}_{1-x}\text{Ge}_x$ buffer layer of a given thickness; this results from a reduction in the surface diffusion length of adatoms caused by greater surface roughness of the buffer layer. As the areal density of the nanoislands increases, the spacing between the islands becomes comparable to their size, and lateral interaction between the elastic-strain fields of neighboring islands can occur. This interaction promotes in-plane ordering of the islands.

Here, we study lateral self-ordering in single layers of SiGe nanoislands grown on strained $\text{Si}_{1-x}\text{Ge}_x$ buffer layers of different thicknesses.

2. EXPERIMENTAL

The structures under study were grown by molecular-beam epitaxy on Si (001) substrates at 700°C. After thermal cleaning of the substrate in the growth chamber and the deposition of a 100-nm-thick Si buffer layer, an additional 10-nm-thick strained $\text{Si}_{1-x}\text{Ge}_x$ layer with the Ge content $x = (0.22 \pm 0.02)$ was grown onto it. The variable thickness of Ge deposited during the formation of nanoislands by the Stranski–Krastanov mechanism was obtained by halting substrate rotation, which ensured a gradient in the amount of deposited Ge from the center to the edge of the substrate. Thus, a Ge layer with an effective thickness varying smoothly across the plane of the structure from 9 to 11 monolayers (MLs) ($1 \text{ ML} = 6.8 \times 10^{14} \text{ atoms/cm}^2 \approx 0.14 \text{ nm}$) was deposited on top of the $\text{Si}_{1-x}\text{Ge}_x$ sublayer.

Measurements of the micro-Raman-scattering spectra were carried out in the backscattering geometry at room temperature using a Horiba Jobin–Yvon T-64000 triple Raman spectrometer equipped with a cooled CCD detector. The 457.9-nm line of an Ar–Kr ion laser was used for excitation; the radiation power was about 1–2 mW, and it was focused onto the sample in a 1- μm -size spot.

High resolution X-ray diffraction (HRXRD) studies of the deformation state and composition of the

grown structures were carried out using an X'PERT PRO MRD diffractometer with a four-crystal monochromator and a three-crystal Ge (220) analyzer; the beam divergence is 12° . In order to investigate the role of elastic stresses and mechanisms of their relaxation in the processes of nanoisland ordering, we measured the reflection curves and the reciprocal-space maps for symmetric and asymmetric diffraction configurations ((004) and (113), (404), respectively). Measurements of the reciprocal-space maps of nanostructures make it also possible to distinguish between the effects of deformations and mosaic structure [11–13].

The morphology of nanoislands was investigated using a Nanoscope IIIa atomic-force microscope (AFM) in the semicontact mode. In order to reduce the distortions introduced due to the finite radius of curvature of the scanning probe, we used TESP-HAR probes (Veeco Inc.) with an apical angle of 5° .

3. RESULTS AND DISCUSSION

To understand the surface morphology of the structures under study, we carried out a statistical analysis of the AFM images of the surface at the control spots corresponding to 9, 10, and 11 MLs of Ge deposited during the process of island formation (Fig. 1). For 9 MLs of Ge, we find a bimodal distribution of the sizes and shapes of the islands, which are of the *hut*-cluster and pyramid types. An increase in the nominal thickness of deposited Ge causes a transition to a unimodal distribution of dome-shaped islands for 10 MLs of Ge and a further narrowing of this distribution for 11 MLs of Ge. A qualitative change in nanostructure morphology is characterized most clearly by the distribution of the island heights. For 9 MLs of deposited Ge, this distribution exhibits two maxima corresponding to heights of 12.9 and 26.6 nm; for 10 and 11 MLs, the height distribution exhibits a single maximum at 37.5 and 37.2 nm, respectively (Fig. 1). The average lateral sizes of islands-pyramids and islands-domes differ slightly and form 220, 208, and 218 nm at thicknesses of the deposited germanium 9, 10, and 11 MLs, respectively.

It should be noted that the areal density of the islands barely changes as the thickness of deposited Ge increases; the density is 27.9, 27.3, and 28.2 μm^{-2} for 9, 10, and 11 MLs of Ge, respectively. Thus, with the areal density of the islands almost constant, the coverage of the surface space with nanoislands increases considerably owing to the complete disappearance of small pyramids and the transformation of large pyramids into domes, which have a larger angle between the side facets and the base.

A decrease in the island spacing leads to a stronger interaction between the islands mediated by the fields of elastic strains generated by them. This elastic interaction causes the effects of spatial ordering in the mutual arrangement of the islands [14]. In the case under study, the ordering effect is fairly evident even in raw AFM images of the structures (Fig. 1). Apart from a more ordered arrangement of the islands, an increase

in the amount of deposited Ge brings about clearer development of the elliptical shape of the island bases, oriented along directions close to $[\bar{1}00]$. To some extent, the anisotropy in the shape of the island base is an indication of the intensity of the elastic interaction between the islands and of the diffusive mass transfer. Thus, for 11 MLs of deposited Ge, the peaks in the distribution of the island orientations (i.e., orientations of the major axes of the ellipses approximating the shape of the island bases) are more pronounced (see Fig. 1); this is evidence for a greater degree of anisotropy of the diffusion processes taking place in the process of island formation. It is also important to note that the two maxima in the island-orientation distributions are separated by $\sim 82^\circ$; i.e., the lateral orientation of the islands deviates somewhat from the $[\bar{1}00]$ and $[010]$ crystallographic directions.

The number and arrangement of peaks in the two-dimensional (2D) autocorrelation functions (Fig. 2) built on the basis of $10 \times 10 \mu\text{m}$ scans give clear evidence of the formation of a characteristic two-dimensional grid in the arrangement of nanoislands. The islands are oriented along directions close to $[010]$ and $[\bar{1}00]$. The occurrence of three peaks in the profiles taken along the two directions shown in Fig. 2b is an indication of short-range order in the mutual arrangement of the islands up to the third-nearest neighbor. This is most pronounced for 10 MLs of deposited Ge; in this case, a fourth-order 2D-autocorrelation peak is observed, which gives evidence of a better-defined periodicity in the island arrangement. The spacing between the peaks in the autocorrelation-function profiles corresponds to the average distance between the islands in a given direction. As the Ge thickness increases, a clear decrease in the period of the island arrangement is observed; along the $[010]$ direction, the period is 200, 188, and 184 nm for 9, 10, and 11 MLs of Ge, respectively.

To understand the role of diffusion during the process of island formation, let us analyze in greater detail the observed increase in the island dimensions with increasing thickness of deposited Ge. It was established from analysis of the AFM data that the amount of material in the islands exceeds the nominally deposited amount of Ge by factors of 3.3 and 5 corresponding to 9 and 11 MLs, respectively. In the case of conventional high-temperature ($\geq 500^\circ\text{C}$) epitaxy on top of a Si buffer, this difference, caused by the diffusion of Si from the buffer layer, can be as large as tens of percent. We demonstrated earlier that the observed effect originates from the anomalously strong diffusion of the alloy atoms from the $\text{Si}_{1-x}\text{Ge}_x$ sublayer to the islands, which causes the net volume of the islands to greatly exceed the total volume of Ge deposited onto the SiGe sublayer [13]. The role of this process becomes more important as the thickness of deposited Ge increases.

Relying on the experimentally determined ratio of the net volume of the islands to the volume of 11 MLs of deposited Ge (which is equal to 5) and taking into

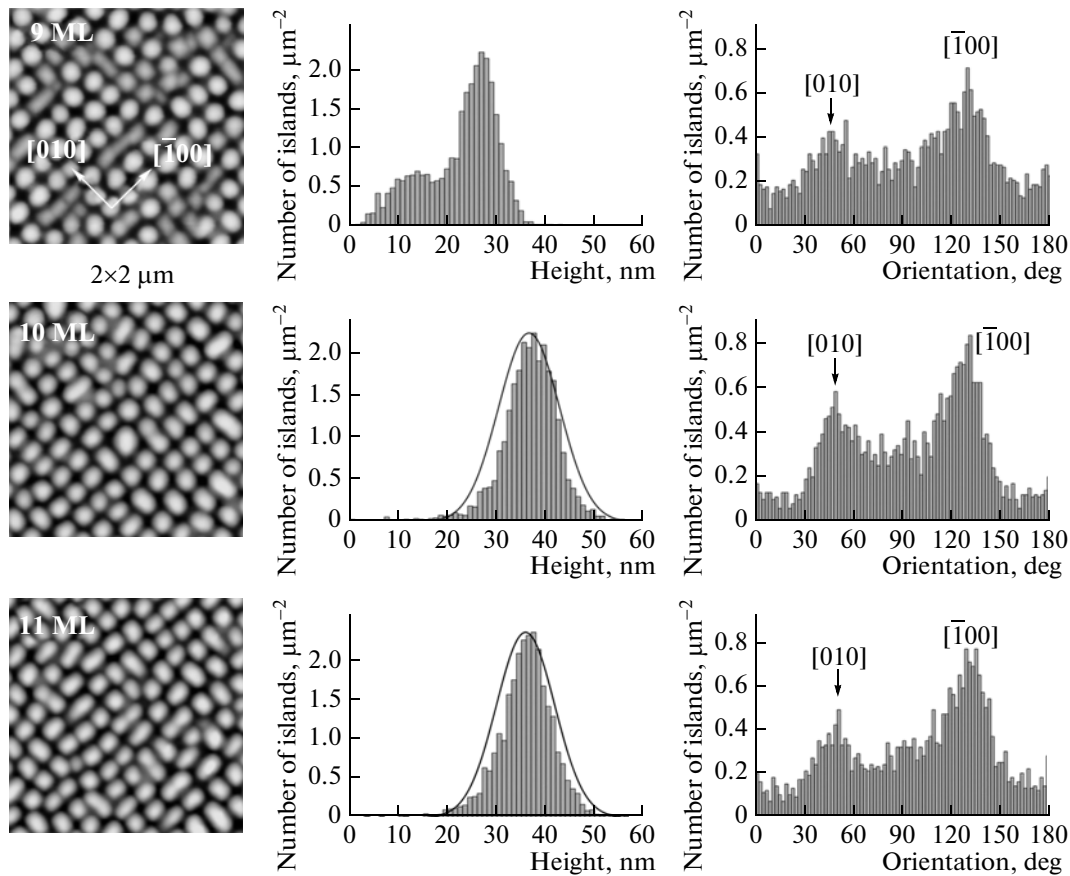


Fig. 1. AFM images of the surface of the structure and histograms for the island heights and the major-axis orientation of the island-base ellipse for 9, 10, and 11 MLs of deposited Ge.

account that, upon growth of the islands on a $\text{Si}_{0.8}\text{Ge}_{0.2}$ sublayer, the thickness of the Ge wetting layer does not exceed 1.5 MLs [12], the net amount of the material that has diffused from the SiGe sublayer to the islands during their growth can be easily estimated. As a result, the following surprising result is obtained. Up to 60% of the strained SiGe buffer sublayer is transferred to the islands. Thus, the thickness of the remaining $\text{Si}_{1-x}\text{Ge}_x$ sublayer in the grown structure is just 3.7 nm, and the net volume of the islands exceeds the volume of the material left in the SiGe sublayer by about a factor of 2. Such a huge flux of diffusing atoms at a temperature considerably lower than the material's melting point can only be explained if we take into account the stimulating role of a nonuniform elastic-strain field (the Gorsky effect [15]), the gradient of which in the studied structures with nanoislands may be very large.

Such strong diffusion of the material into the islands during the process of their formation leads to considerable changes in the nominal composition of the layers and strains in the system. It is also evident that the kinetics of this process considerably affects the resulting structural morphology.

Micro-Raman spectroscopy was applied to determine the composition and strain in the structure under study. The Raman spectra (see Fig. 3) exhibit bands corresponding to Si–Si, Si–Ge, and Ge–Ge vibrations, which is typical of Ge/Si structures with nanoislands [16–18]. The difference from conventional cases of islands grown on a Si buffer lies in the doublet character of the bands, which manifests itself most clearly for the Si–Si band at 11 MLs of Ge. As we demonstrated previously [13], this is related to the presence of two regions of the SiGe alloy with different compositions and which are differently strained; these regions are the islands and the $\text{Si}_{1-x}\text{Ge}_x$ sublayer. The broader low-frequency component of the doublet corresponds to the islands and the narrower high-frequency component corresponds to the SiGe underlayer. From a decomposition of the Si–Si and Si–Ge vibration bands into their components, we estimated the composition and strain for the $\text{Si}_{1-x}\text{Ge}_x$ sublayer and the islands (Table 1) using the procedure described in [19].

The results listed in Table 1 confirm the occurrence of anomalously strong diffusion of the material into the islands. Thus, considerable redistribution of the material between the islands and the buffer sublayer

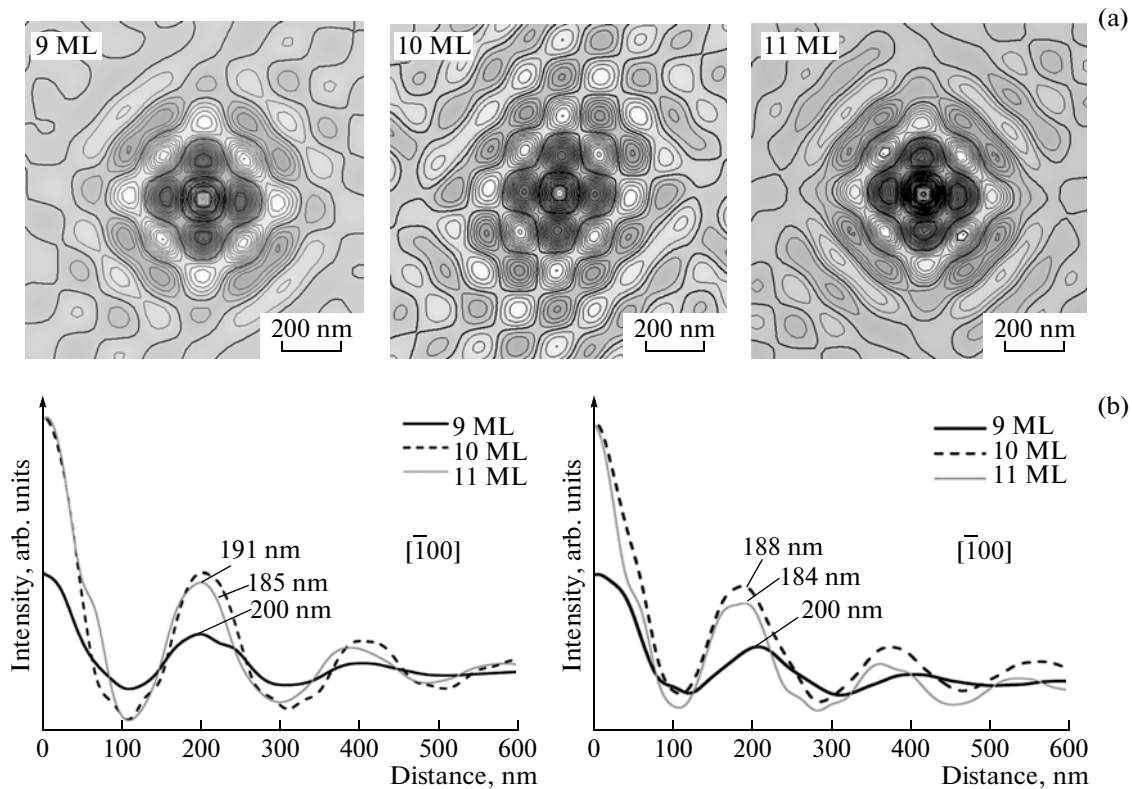


Fig. 2. (a) Autocorrelation maps obtained from AFM scans of the structures under study for 9, 10, and 11 MLs of deposited Ge. (b) Profiles of the autocorrelation maps along the directions $[010]$ and $[\bar{1}00]$.

leads to an increase in the Ge content in the sublayer and almost complete strain relaxation in the islands. Since the lattice constant of Ge exceeds that of Si by 4%, this should cause an increase in the elastic energy of the sublayer; apparently, this fact makes the above result unlikely. However, this conclusion would be valid if the thickness of the SiGe layer were constant.

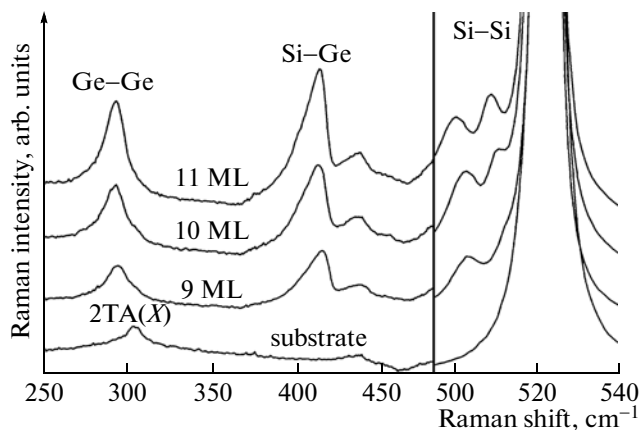


Fig. 3. Room-temperature Raman spectra of the structure under study for 9, 10, and 11 MLs of deposited Ge. The excitation wavelength $\lambda = 457.9$ nm.

The elastic energy accumulated in the layer is proportional to its thickness d and the square of the ε_{xx} component of the deformation tensor: $E \propto \varepsilon_{xx}^2 d$. Thus, the elastic energy of the $\text{Si}_{1-x}\text{Ge}_x$ sublayer remains constant if the observed 1.5-fold increase in the Ge content is accompanied by a reduction in the layer thickness by at least a factor of 2.25, i.e., to 4.4 nm. Above, we obtained an estimate $d_1 = 3.7$ nm, which is in agreement with this requirement; actually, this result means that the diffusion of the alloy atoms from the SiGe layer brings about a decrease in its elastic energy. Comparing the changes in the thickness and composition of the buffer layer, one can easily estimate the relationship between the amounts of Si and Ge atoms transferred out of the buffer layer. It proves that the fraction of Ge atoms in the net flux of atoms transferred from the buffer to the islands is $\sim 16\%$.

This result supports the above conclusion that the main driving force of the diffusion process under discussion is the Gorsky effect. This effect stimulates the diffusion of Si atoms into the islands and, simultaneously, supports uphill diffusion of Ge atoms from the SiGe sublayer, where the Ge content is lower, to the islands, where the Ge content is initially much higher.

The considerable increase in the Si content in the islands as compared to the previously studied nanostructures obtained by the epitaxy of Ge on Si under similar technological modes (i.e., at 700°C and for 11 MLs of deposited Ge) should be noted. This fact is readily understood, taking into account that the replacement of a Si buffer layer by a SiGe layer leads to a decrease in the critical thickness of the Ge layer corresponding to the transition from two-dimensional to three-dimensional growth [11, 12]. As a consequence, the process of island growth takes longer and, thus, the time available for the material to diffuse from the buffer to the islands increases as well. Still more important is the fact that a smaller thickness of the Ge wetting layer facilitates the diffusion of atoms from the SiGe sublayer to the islands.

Next, the ordering of the islands was investigated by HRXRD, which represents a nondestructive method for studying multilayer nanostructures [20–22]. This method yields information on the strain conditions and degree of spatial ordering in nanostructures [23]. It has been successfully applied to studies of the spatial ordering of QDs in various systems, such as PbSe/PbEuTe [24], InGaAs/GaAs [25], and Si/Ge [26].

For the control spots of the structure under study, rocking curves on the asymmetrical reflections were recorded. (113) and (404) scans for the {110} and {100} diffraction planes were performed. This experimental configuration makes it possible to determine the lattice constants in the directions perpendicular and parallel to the surface and the composition of the structure under study [21, 22]. Lateral satellites are clearly seen in the rocking curves (Fig. 4), which is evidence of ordering in the system of SiGe islands. The average spacing between the diffuse peaks on these curves yields information on the average spacing between the islands along the [110] direction (from the (113) reflection) and the [100] and [010] directions (from mutually orthogonal (404) reflections). The values of the lateral period thus obtained for the three control spots on the sample are listed in Table 2. These data clearly demonstrate that the QD spacing along the [100] and [010] directions is different; i.e., the lateral unit cell of the island array is not strictly orthogonal.

To reveal factors responsible for the observed features of the lateral ordering of the islands we analyzed the influence of the substrate orientation on the island arrangement along crystallographic directions. The substrate was slightly misoriented in a direction close to [010], so that the misorientation angles are $\sim 0.4^\circ$ in the $[\bar{1}\bar{1}0]$ direction and 0.3° in the $[\bar{1}10]$ direction. Meanwhile, the SiGe buffer layer is only misoriented along the $[\bar{1}10]$ direction by 0.2° . As we demonstrated previously [21], this kind of misorientation of a SiGe layer on a tilted substrate is caused by anisotropic deformation of its crystal lattice. The absence of misorientation along another direction may indicate that

Table 1. Ge content and strain in the sublayer and the islands determined from Raman spectra

Ge thickness	Sublayer		Islands	
	x	ε_{xx}	x	ε_{xx}
9 MC	0.30	−0.014	0.29	−0.003
10 MC	0.32	−0.013	0.31	−0.001
11 MC	0.33	−0.012	0.32	0.001

Table 2. Lateral period (in nm) in the island arrangement along different crystallographic directions according to X-ray diffraction data

Ge thickness	113 (0°)	113 (90°)	404 (45°)	404 (−45°)
9 MC	260	269	177	164
10 MC	255	246	172	—
11 MC	226	226	165	157

Note: The values of zone are given in nm.

it is partially compensated on account of the appearance of a deviation of the opposite sign along the [110] direction, which is caused by a decrease in the buffer-layer thickness with increasing Ge content.

According to [27], for $0.2 < x < 0.6$ the growth of a planar $\text{Si}_{1-x}\text{Ge}_x$ layer on a Si substrate preceding the formation of faceted islands is accompanied by the appearance of an ordered pattern in the form of a network of roughnesses with a characteristic period from 100 to 200 nm depending on x . This effect was attributed to the energy gain upon the appearance of growth instabilities induced by the elastic strains. Apparently,

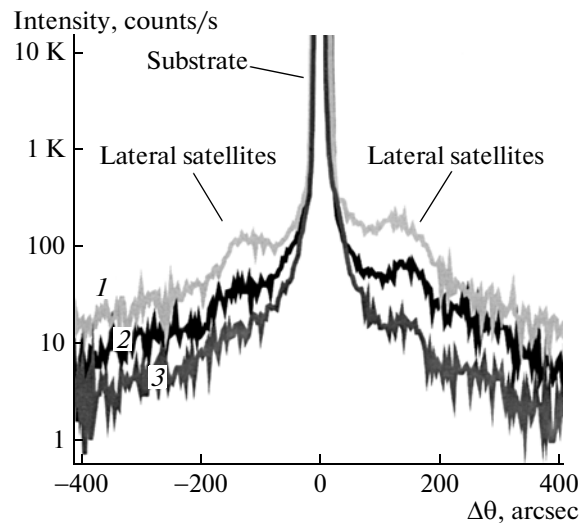


Fig. 4. X-ray diffraction ω -scans of the structure under study for (1) 9, (2) 10, and (3) 11 MLs of deposited Ge.

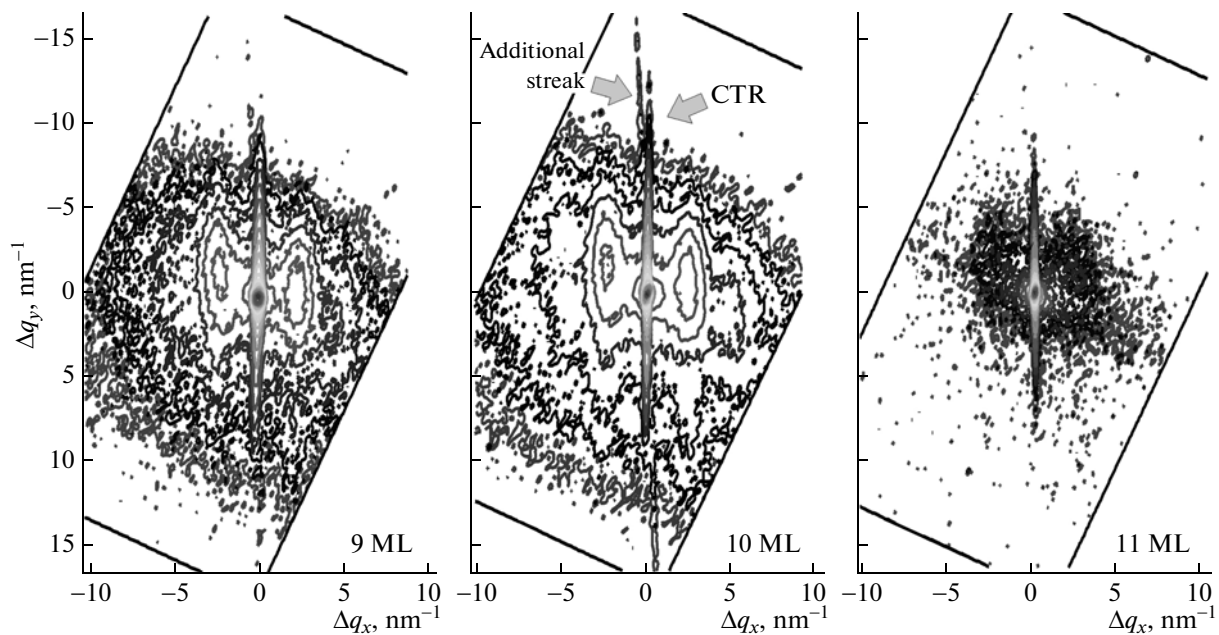


Fig. 5. Reciprocal space maps obtained in the (113) asymmetric diffraction configuration for 9, 10, and 11 MLs of deposited Ge.

the formation of such a pattern is accompanied by the modulation of elastic surface strains in the structure.

When a strained $\text{Si}_{1-x}\text{Ge}_x$ layer is grown on a misoriented Si surface, additional periodic modulation of the strain in the plane of the structure will appear. As the Ge content in the buffer layer increases, the layer misorientation increases as well, which causes larger modulated strains along the surface [28]. Thus, for Si/Si_{1-x}Ge_x multilayer structures grown on slightly misoriented Si surfaces, the formation of a periodic wave-like pattern along the direction of the substrate tilt was observed [29–31]. The characteristic lateral period of the modulation pattern exceeded the atomic-step spacing on the misoriented substrate by a large factor.

Thus, it is reasonable to suggest that nucleation and spatial ordering of nanoislands on a misoriented Si_{1-x}Ge_x sublayer is governed by this modulation pattern and the corresponding nonuniform elastic-strain fields. Due to the modulation, places favorable for island nucleation will appear on the surface of the structure. The nonuniform field of elastic strains originating in the Si_{1-x}Ge_x sublayer will also affect the growth of nanoislands, bringing about anisotropy in their shape and spatial arrangement.

The degree of QD ordering is enhanced as the thickness of deposited Ge increases from 9 to 10 MLs. This is evidenced by the appearance of second-order lateral satellites in the diffraction curves and reciprocal-space maps, which correlates with the AFM data (Fig. 1). For 11 MLs of Ge these satellites disappear. The blurring of the satellites, accompanied by an enhancement of the general diffuse background, may be explained by deterioration in the structural perfec-

tion of the system as a whole. In particular, this effect can take place due to the partial coalescence of neighbouring islands (i.e., the formation of defective islands) (Fig. 5).

According to Table 2, the lateral period of the island arrangement decreases with increasing thickness of deposited Ge. This fact correlates with the increase in the coverage of the surface by the islands, observed in the AFM images, and the results obtained from analysis of the autocorrelation maps. Analysis of the (113) and (404) reflections demonstrates that there is a small difference in the neighboring-island spacing along two mutually perpendicular directions. This observation is indicative of an ordered island arrangement in the form of a lateral periodic pattern whose unit cell differs slightly from a square.

Detailed information on the parameters of the structures under study can be obtained from the reciprocal-space maps recorded for different reflections and different sample orientations. Reciprocal space maps recorded for (113) and (404) asymmetric configurations support our understanding of the character of island ordering at different points along the length of the sample (see Fig. 5). The most ordered arrangement was observed for 10 MLs of deposited Ge, the least ordered was observed for 11 MLs. Indeed, the reciprocal space maps recorded for the (113) reflection in the case of 10 MLs of Ge contain an additional band oriented at a small angle to the main reflection (labeled as CTR). We believe this diffraction effect is a result of the specular reflection of the X-ray beam from the island facets. This additional band is absent in the maps obtained for 9 and 11 MLs of Ge, since there is no reflection from the island facets in these cases.

Thus, the case of 10 MLs of deposited Ge does correspond to the most ordered arrangement of the islands and their most uniform distribution in terms of size and shape.

X-ray analysis data confirmed that elastic-strain relaxation did not occur in any of the deposited $\text{Si}_{1-x}\text{Ge}_x$ buffer layers. Thus, the supposed decrease in the surface diffusion length of Ge adatoms cannot be a consequence of a change in the lattice constant; independent of the Ge content, the in-plane lattice constant of the deposited strained $\text{Si}_{1-x}\text{Ge}_x$ layers remained equal to the lattice constant of bulk Si.

A somewhat unusual position of lateral satellites with respect to the peak of the substrate should be noted as well. Projected onto the diffraction vector, they appear at larger angles, i.e., in the region of smaller lattice parameters. This seems rather strange in view of the larger atomic-plane spacing in the SiGe alloy layer on the Si substrate.

4. CONCLUSIONS

We have investigated spatial ordering in single layers of Ge islands obtained by depositing different amounts of Ge on a strained $\text{Si}_{1-x}\text{Ge}_x$ sublayer. It is demonstrated that an increase in the effective thickness of Ge stimulates spatial ordering of the islands that results from stronger interaction between the elastic-strain fields of neighboring islands, which is brought about by an increased coverage of the surface space by the islands. The presence of spatially nonuniform elastic-strain fields induced by misorientation of the substrate and the buffer layer leads to the enhanced importance of interdiffusion processes causing an anomalously intense atomic flux from the buffer sublayer to the islands, in which partial relaxation of elastic strains takes place. The resulting morphology of self-assembled nanostructures is determined by the kinetics of this process, and the total volume of the islands may be several times larger than the volume of deposited Ge. The anisotropic character of the diffusion processes occurring during the process of structure formation gives rise to anisotropy in the shape and mutual arrangement of the islands. For the deposition temperature used, the most ordered arrangement of the islands has been observed for an effective thickness of deposited Ge equal to 10 MLs. As the amount of deposited Ge is increased further, the ellipticity in the shape of the island bases becomes more pronounced.

ACKNOWLEDGMENTS

This study was supported by the State Science and Technology Program of Ukraine “Nanotechnologies and nanomaterials” (project nos. 3.5.2.6 and 3.5.1.12/19), the State Fund for Fundamental Researches of Ukraine (project no. F38/363), and the Ministry of Education and Science of Ukraine (project no. M90/2010).

REFERENCES

1. J. Philips, *J. Appl. Phys.* **91**, 4590 (2002).
2. V. A. Shchukin, N. N. Ledentsov, and D. Bimberg, in *Epitaxy of Nanostructures*, Ser. Nanoscience and Technology (Springer, 2004), p. 387.
3. D. Leonard, M. Krishnamoorthy, C. M. Reaves, S. P. Denbaars, and P. M. Petroff, *Appl. Phys. Lett.* **63**, 3203 (1993).
4. G. Abstreiter, P. Schittenhelm, C. Engel, E. Silveira, A. Zrenner, D. Meertens, and W. Jäger, *Semicond. Sci. Technol.* **11**, 1521 (1996).
5. A. Bernardi, M. I. Alonso, A. R. Goñi, J. O. Ossö, and M. Garriga, *Appl. Phys. Lett.* **89**, 101921 (2006).
6. Yu. B. Bolkhovityanov, O. P. Pchelyakov, and L. V. Sokolov, *Semiconductors* **37**, 493 (2003).
7. Z. Zhong, H. Lichtenberger, G. Chen, M. Muhlberger, C. Schelling, J. Myslivecek, A. Halilovic, J. Stangl, G. Bauer, W. Jantsch, and F. Schaffler, *Microelectron. Eng.* **83**, 1730 (2006).
8. I. Berbezier, M. Descoins, B. Ismail, H. Maaref, and A. Ronda, *J. Appl. Phys.* **98**, 063517 (2005).
9. D. N. Lobanov, A. V. Novikov, N. V. Vostokov, Y. N. Drozdov, A. N. Yablonskiy, Z. F. Krasilnik, M. Stoffel, U. Denker, and O. G. Schmidt, *Opt. Mater.* **27**, 818 (2005).
10. N. V. Vostokov, Yu. N. Drozdov, Z. F. Krasilnik, D. N. Lobanov, A. V. Novikov, and A. N. Yablonskii, *Phys. Solid State* **41**, 42 (2005).
11. D. V. Yurasov and Yu. N. Drozdov, *Semiconductors* **42**, 563 (2008).
12. D. V. Yurasov, Yu. N. Drozdov, M. V. Shaleev, and A. V. Novikov, *Appl. Phys. Lett.* **95**, 151902 (2009).
13. M. Ya. Valakh, P. M. Lytvyn, A. S. Nikolenko, V. V. Strelchuk, Z. F. Krasilnik, D. N. Lobanov, and A. V. Novikov, *Appl. Phys. Lett.* **96**, 141909 (2010).
14. N. V. Vostokov, Yu. N. Drozdov, Z. F. Krasilnik, D. N. Lobanov, A. V. Novikov, A. N. Yablonskii, M. Stoffel, U. Denker, O. G. Schmidt, O. M. Gorbenko, and I. P. Soshnikov, *Phys. Solid State* **47**, 26 (2005).
15. Ya. E. Geguzin, *Sov. Phys. Usp.* **29**, 467 (1986).
16. A. Bernardi, M. I. Alonso, J. S. Reparaz, A. R. Goñi, P. D. Lacharmoise, J. O. Osso, and M. Garriga, *Nanotechnology* **18**, 475401 (2007).
17. M. I. Alonso, M. de la Calle, J. O. Ossö, M. Garriga, and A. R. Goñi, *J. Appl. Phys.* **98**, 033530 (2005).
18. J. S. Reparaz, A. Bernardi, A. R. Goñi, M. I. Alonso, and M. Garriga, *Appl. Phys. Lett.* **92**, 081909 (2008).
19. V. S. Lysenko, Yu. V. Gomeniuk, V. V. Strelchuk, A. S. Nikolenko, S. V. Kondratenko, Yu. N. Kozyrev, M. Yu. Rubezhanska, and C. Teichert, *Phys. Rev. B* **84**, 115425 (2011).
20. V. P. Kladko, L. I. Datsenko, J. Bak-Misiuk, S. I. Olikhovskii, V. F. Machulin, I. V. Prokopenko, V. B. Molodkin, and Z. V. Maksimenko, *J. Phys. D: Appl. Phys.* **34**, A87 (2001).
21. O. Yefanov, V. Kladko, O. Gudymenko, V. Strelchuk, Yu. Mazur, Zh. Wang, and G. Salamo, *Phys. Status Solidi A* **203**, 154 (2006).

22. Yu. I. Mazur, Z. M. Wang, G. J. Salamo, V. V. Strelchuk, V. P. Kladko, V. F. Machulin, M. Ya. Valakh, and M. O. Manasreh, *J. Appl. Phys.* **99**, 023517 (2006).
23. J. Stangl, V. Holy, and G. Bauer, *Rev. Mod. Phys.* **76**, 725 (2004).
24. G. Springholz, V. Holy, M. Pinczolits, and G. Bauer, *Science* **282**, 734 (1998).
25. V. Kladko, M. Slobodian, P. Lytvyn, V. Strelchuk, Yu. Mazur, E. Marega, M. Hussein, and G. Salamo, *Phys. Status Solidi A* **206**, 1748 (2009).
26. V. Holy, A. A. Darhuber, J. Stangl, G. Bauer, J. Nutzeland, and G. Abstreiter, *Phys. Rev. B* **57**, 12435 (1998).
27. R. M. Tromp, F. M. Ross, and M. C. Reuter, *Phys. Rev. Lett.* **84**, 4641 (2000).
28. A. Sanz-Hervás, M. Aguilar, J. L. Sánchez-Rojas, A. Sacedón, E. Calleja, E. Muñoz, C. Villar, E. J. Abril, and M. López, *J. Appl. Phys.* **82**, 3297 (1997).
29. Y. H. Phang, C. Teichert, M. G. Lagally, L. J. Peticolos, J. C. Bean, and E. Kasper, *Phys. Rev. B* **50**, 14435 (1994).
30. P. Sutter and M. G. Lagally, *Phys. Rev. Lett.* **84**, 4637 (2000).
31. M. Meduna, V. Holy, T. Roch, G. Bauer, O. G. Schmidt, and K. Eberl, *J. Phys. D: Appl. Phys.* **34**, A193 (2001).

Translated by M. Skorikov